JOURNAL OF MATERIALS SCIENCE 19 (1984) 2696–2704

Spherulites and phase separation in plasma–dissociated zircon

R. McPHERSON, B. V. SHAFER
Department of Materials Engineering, Monash University, Clayton, Victoria, 3168, Australia

Plasma-dissociated zircon consists of a mixture of monoclinic and tetragonal ZrO_2 in SiO_2 glass. The proportion of tetragonal ZrO_2 increases with decreasing initial zircon particle size and increasing cooling rate; zircon sprayed onto a cold substrate consists entirely of tetragonal ZrO_2 in glass. Tetragonal ZrO_2 is nucleated at large undercooling during cooling of molten zircon particles and grows in a spherulitic manner because of a low-diffusivity boundary layer at the growing crystal–liquid interface. At smaller particle sizes and higher cooling rates the thermal history of liquid droplets is such that an alternative process of phase separation into ZrO_2-rich and SiO_2-rich liquids becomes possible in the liquid remaining between spherulites. The particle size distribution of the ZrO_2 crystallites which form in this way shifts towards smaller particle sizes with increasing cooling rate and those smaller than ~ 20 nm diameter do not transform to the equilibrium monoclinic form on cooling to room temperature because of a surface/matrix restraint effect.

1. Introduction

As long ago as 1931 it was reported that zircon ($ZrSiO_4$), melted in an electric arc furnace, formed a mixture of fibrous monoclinic ZrO_2 in a SiO_2 rich glass on cooling [1].

George and Lambert [2] also reported the complete dissociation of zircon into ZrO_2 crystals and SiO_2 glass by melting followed by rapid cooling, and pointed out that dissociation was much less extensive if zircon was heated below its melting temperature. This is supported by experiments conducted by Curtis and Sowman [3] who observed that heating for six hours at 1760° C was required for complete dissociation of zircon. A phase diagram for the ZrO_2–SiO_2 system, based on their results, showed dissociation of zircon into ZrO_2 and SiO_2 below the liquidus (~ 1540° C), and the formation of ZrO_2 and a SiO_2-rich liquid at temperatures greater than 1680° C. The phase diagram now generally accepted is based on that of Butterman and Foster [4] which shows an upper limit of zircon stability of 1676° C, just below the temperature at which a liquid phase is formed (1687° C). This diagram also shows liquid immiscibility above 2250° C.

A 1965 review of applications of plasma technology in extractive metallurgy [5] suggested the possibility of using a plasma reactor to dissociate zircon. Later experiments in which zircon particles were passed through a high frequency plasma [6] demonstrated that plasma dissociation into ZrO_2 crystals and SiO_2 glass was possible. Microscopic examination of the spheriodized particles showed evidence of radial growth of small ZrO_2 crystals, described as dendritic, in glass. X-ray diffraction suggested that the product contained "pseudo-cubic" ZrO_2; however, the sample examined was a ZrO_2 enriched material taken from the inside of the plasma confining tube and may have consisted of a very fine condensation product.

More recently commercial [7] and pilot scale [8] plasma dissociation of zircon has been reported. These processes have involved the injection of a stream of zircon concentrate particles through a large volume plasma (100 to 300 kw) so that they rapidly melt and resolidify. The

0022–2461/84 $03.00 + .12

product, referred to as plasma dissociated zircon (PDZ), is a convenient starting point for the preparation of ZrO_2 powder since the SiO_2 phase can be readily removed by leaching with NaOH.

Several studies of commercially prepared PDZ have shown that it consists of monoclinic ZrO_2 crystals dispersed in a SiO_2 rich glass [9–11]. Cellular microstructures observed on the surface of some PDZ particles were at first described as recrystallized grains because of their similarity to the grains of a polycrystalline metal [9]. Droplet structures of spherical ZrO_2 crystals dispersed in glass suggested that metastable phase separation could be a significant factor in microstructural development if crystallization of primary ZrO_2 was suppressed by large undercooling [11]. More recently Wong and McPherson [12] have suggested that the predominant radial crystal growth pattern of monoclinic ZrO_2 in PDZ is spherulitic in nature and arises from diffusion-controlled growth in the viscous silicate liquid. The various transverse dimensions of the spherulitic crystal arms thus arise from growth at different temperatures in accordance with the theory of spherulitic growth advanced by Keith and Paddern [13]. It was also proposed that droplet structures may arise from phase separation in SiO_2-enriched intercrystalline liquid, and that some of the ZrO_2 particles formed in this way may be sufficiently small to persist as the tetragonal form on cooling because of the well known particle size stabilisation effect [14].

The structure of zircon which has been melted and rapidly cooled is also of interest in sprayed coating technology and Ault [15] reported that a flame sprayed zircon coating consisted of a dispersion of cubic ZrO_2 in glass. Krauth and Meyer [16], however, observed that plasma sprayed zircon coatings contained a mixture of the monoclinic and tetragonal forms of ZrO_2. X-ray line broadening analysis suggested that the tetragonal crystallites were smaller than approximately 18 nm in size and annealing above 900° C resulted in crystal growth and transformation to the monoclinic form. Zircon was reformed if the coating was heated to between 1400 and 1600° C. Japanese workers [17] have reported similar results but also found that a product consisting entirely of tetragonal ZrO_2 in glass could be formed by spraying onto a water-cooled substrate.

Although PDZ is usually referred to as being rapidly quenched [9], previous studies of the structure of spheroidized oxides have shown that the particle size is of major importance in determining the thermal history of plasma-processed materials and hence the structure finally observed [18]. The furnace configurations generally used for PDZ production are designed to give high conversion efficiencies at large throughputs, by using large plasma volume and low particle velocity, resulting in a relatively low cooling rate. The present paper is concerned with the structure of PDZ prepared by means of a large scale plasma reactor as well as material prepared using much higher cooling rates achieved by a small particle feed size and a compact plasma device.

2. Experimental

Australian zircon sand, ground to $-53\,\mu m$ particle size, was separated into the following narrow size fractions using a Cyclosizer elutriation apparatus followed by a continuous flow centrifuge: $-53+29$, $-29+22$, $-22+16$, $-16+11$, $-11+6$ and $-6\,\mu m$. Various fractions were spheroidized using a plasma apparatus based on a previously described design [19]. Briefly this consisted of a d.c. plasma torch operating within a circular cross-section, closed reaction chamber into which a stream of quenching gas, usually He, could be injected radially (perpendicular to the plasma jet) 150 mm downstream from the plasma torch orifice. The powder to be treated was injected, as a suspension in N_2, into the plasma jet within a few mm of the torch orifice. The spheroidized product was collected by means of a cyclone in the gas stream approximately 200 mm downstream from the quenching gas injection point following a convergent section of the reaction chamber. Experiments were conducted with plasma torch power inputs of 14 to 25 kW using N_2–H_2 gas mixtures. Some samples were also prepared by plasma spraying thin layers (~0.1 mm) onto cold aluminium substrates. A sample of PDZ prepared at the National Physical Laboratory (NPL) using a 100 kW pilot scale apparatus [8] was also studied.

Processed powders were examined by X-ray diffraction using Cu$K\alpha$ radiation in a Philips diffractometer. The relative proportions of tetragonal ZrO_2, monoclinic ZrO_2 and zircon were estimated from the integrated intensities of the $(1\,1\,1)$ and $(1\,1\,\bar{1})$ monoclinic, the $(1\,1\,1)$ tetragonal line and the $(1\,0\,1)$ zircon lines scanned at $1/8°\ min^{-1}$. The relative proportions of tetragonal and monoclinic forms of ZrO_2 may be found [20], within an error of ~5%, from the relationship:

$$I_{m(111)} + I_{m(11\bar{1})} = I_{t(111)}$$

This relationship was also used to estimate the proportion of zircon by determining the ratio of the integrated intensities of the (101) zircon line to the sum of the intensities of the (111) and $(11\bar{1})$ monoclinic and (111) tetragonal lines. Known mixtures of zircon and PDZ were used to determine a calibration curve.

ZrO_2 crystallite sizes were estimated from the line breadth, at half peak height, using the relationship:

$$D = \lambda/\beta \cos\theta \qquad (1)$$

where D is crystallite diameter, λ is wavelength of radiation, θ is diffraction angle and β is corrected line breadth using the correction curve appropriate for the diffractometer configuration [21]. This assumes negligible strain broadening, a reasonable assumption in the present circumstances for isolated tetragonal ZrO_2 crystallites in a SiO_2 matrix, since any thermal strain arising from differential thermal contraction between ZrO_2 and SiO_2 would result only in an overall shift of the diffraction lines.

The microstructure of PDZ was examined by scanning electron microscopy (SEM) and transmission electron microscopy (TEM). SEM of the external surfaces of PDZ spheres and also the interior fracture surfaces of broken spheres made use of a Cambridge stereoscan microscope fitted with a back scattered electron detector to provide atomic number contrast. Specimens for TEM, using a JEOL 100C microscope, were prepared by ion beam thinning of PDZ particles attached to Cu microscope grids using epoxy resin. Some specimens partly thinned in the same way were also used for SEM to provide an indication of the internal microstructure.

3. Results

X-ray diffraction of the spheroidized powders revealed that they consisted of a mixture of tetragonal and monoclinic ZrO_2, the proportion of tetragonal phase increasing with decreasing feed powder particle size as shown in Fig. 1. Zircon was only detected in samples of the $-53 + 29\,\mu m$ fraction treated at plasma powers less than ~ 15 kW; all further discussion will be related only to PDZ in which zircon could not be detected by X-ray diffraction. The quenching gas flow rate had a secondary effect at particle sizes larger than $\sim 11\,\mu m$ and the influence of quench gas flow

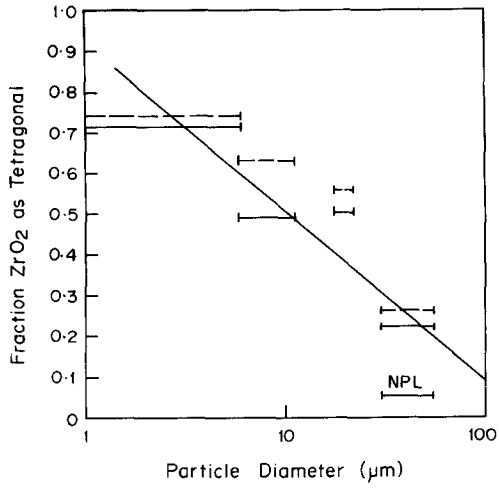

Figure 1 Fraction tetragonal ZrO_2 as a function of initial zircon particle size. Dashed lines correspond to higher quench gas rates than full lines.

rate on the proportion of tetragonal phase in the $-11\,\mu m$ fractions was not reproducible, probably due to particle recirculation within the reaction chamber. The very much lower proportion of tetragonal ZrO_2 in the $-53 + 37\,\mu m$ fraction of the NPL sample of PDZ [18] is shown for comparison with the same size powder treated in the present apparatus. The proportion of tetragonal ZrO_2 in treated powders was significantly reduced by mechanical grinding as reported for other examples of metastable tetragonal ZrO_2 [22, 23].

X-ray line broadening determinations of the crystallite size of the tetragonal ZrO_2 phase gave a mean of ~ 20 nm for all powders examined.

SEM, using a back scattered electron detector to provide atomic number contrast, clearly shows the spherulitic growth pattern of ZrO_2 crystals (white) in a SiO_2 glass matrix (black) on the surface of PDZ as previously reported [12]. A range of spherulite morphologies was observed as illustrated in Figs. 2 and 3.

Fig. 2a illustrates the case in which the surface of a $+29, -53\,\mu m$ laboratory-prepared particle consists entirely of small ZrO_2 spherulites ($\sim 4\,\mu m$ diameter) in a SiO_2 glass matrix whereas another particle from the same sample has $\sim 2\,\mu m$ diameter spherulites dispersed within an unresolved (grey) matrix (Fig. 2b). A dark band, that is a predominantly SiO_2 glass rim, may be observed around the spherulites. Fig. 3a shows the surface of an NPL particle in which well-developed ZrO_2 spherulites ($\sim 12\,\mu m$ diameter) are observed with a distinct circular ZrO_2 particle at the centre of each spheru-

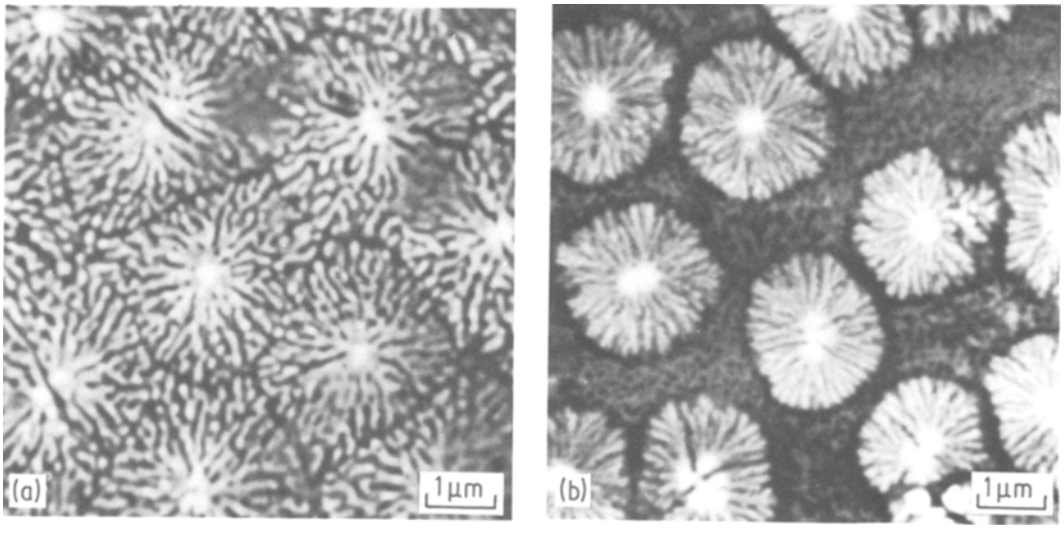

Figure 2 SEM, surfaces of + 29, − 53 μm fraction laboratory prepared PDZ particles.

lite. The region surrounding the spherulites apparently consists of small isolated ZrO_2 particles in SiO_2 glass and some "cloudy" regions in which the structure is unresolved. A somewhat similar structure is observed in another NPL particle (Fig. 3b) but in this case there are also irregularly shaped light regions containing dark circular particles present.

An examination of fractured PDZ particles (Fig. 4) revealed that the spherulitic ZrO_2 in SiO_2 glass structures occurred throughout. This figure also shows a thin layer, which is partly transparent to the electron imaging system, on the surface of an internal pore. EDAX analysis showed the presence of Si only and the material is tentatively identified as condensed SiO. Examination of the surface of an ion-beam thinned particle also confirms that the spherulitic structure occurs throughout the particle volume (Fig. 5). TEM of ion-beam thinned foils of NPL particles shows cross-sections of the twinned monoclinic ZrO_2 spherulite arms with SiO_2 glass between them (Fig. 6a). However, in some regions the glass contains small spherical particles which selected-area diffraction shows to be randomly oriented tetragonal ZrO_2 crystals (Fig. 6b). The observation that the twins are parallel in many of the ZrO_2 regions emphasizes the non-crystallographic branching typical of

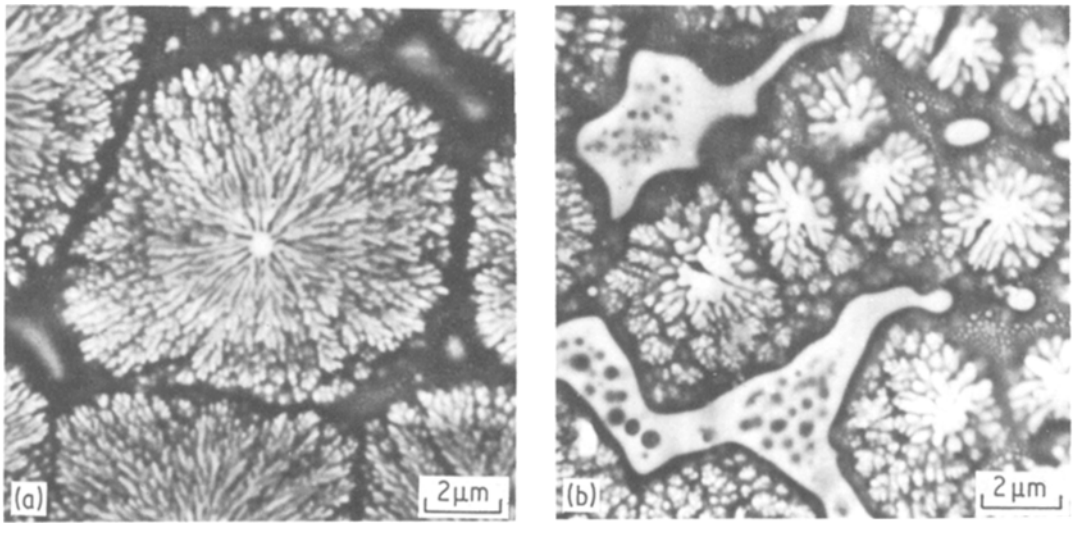

Figure 3 SEM, surfaces of NPL PDZ particles.

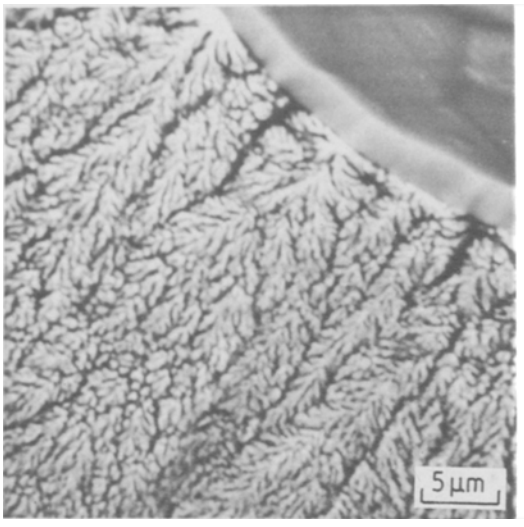

Figure 4 SEM, fracture surface of NPL PDZ particle.

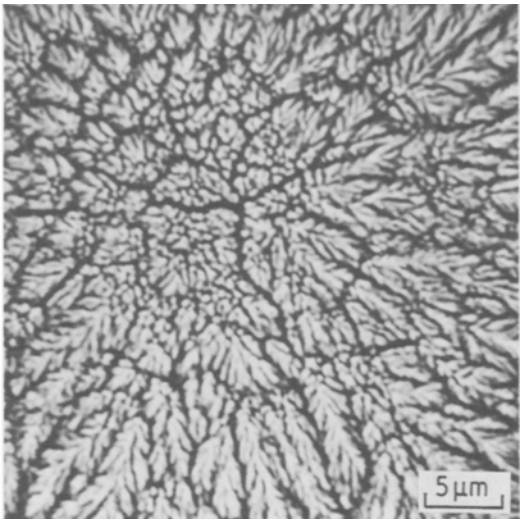

Figure 5 SEM, ion beam thinned surface of NPL PDZ particle.

spherulitic structures. Other regions of the PDZ (Fig. 6c) show a range of sizes of spherical ZrO_2 particles dispersed in glass, in some cases the larger spheres contain lighter regions within them.

TEM of $\sim 10\,\mu m$ diameter laboratory prepared material shows large regions which consist only of a range of ZrO_2 particles in glass, with the smallest particles < 10 nm diameter (Fig. 7a). Very thin regions of some of the foils prepared from this powder showed an extremely fine modulated substructure (Fig. 7b) which was shown, by selected area diffraction (Fig. 7c), to consist of extremely fine crystals of tetragonal ZrO_2 in glass. A similar microstructure was observed in a sample of zircon sprayed onto a cold substrate.

4. Discussion

The SEM studies show that the predominant structure of the NPL and the larger laboratory prepared PDZ consists of spherulites of monoclinic ZrO_2 in SiO_2 glass. Some of the interspherulite regions of both types of PDZ have a microstructure consisting of a very fine dispersion of monoclinic and tetragonal ZrO_2 crystals in glass. The X-ray diffraction data show that the proportion of ZrO_2 present in the fine tetragonal dispersion increases as the initial particle size decreases until, with the finest powders, the structure consists almost entirely of the dispersed structure. Although it was not possible to prepare TEM foils which were known to cover the interspherulitic regions, it seems quite clear that the microstructures consisting of dispersed particles of monoclinic and tetragonal ZrO_2 in glass observed by TEM correspond with the cloudy regions observed by SEM.

The X-ray data show that the tetragonal phase has a crystallite size of about 20 nm which is consistent with the finest particles observed by TEM in the PDZ and sprayed coating; this figure is also in agreement with Krauth and Meyer's study [16]. The stabilisation of tetragonal ZrO_2 at small particle sizes is a function of the matrix, thus the critical size is approximately 10 nm for isolated particles [14], 600 nm in cubic ZrO_2 solid solutions [24], 150 nm in zircon [25] and 1 μm in Al_2O_3 [26]. The critical size in SiO_2 glass, from the present study, is approximately 20 nm, consistent with the lower restraint to the tetragonal–monoclinic transformation provided by the low elastic modulus of this matrix compared with ZrO_2, zircon and Al_2O_3.

The increase in the proportion of tetragonal ZrO_2 as the particle size of the PDZ is reduced (and/or cooling rate increased) is thus related to a change in the ZrO_2 particle size distribution towards smaller diameters. Large particle size PDZ produced in a commercial scale reactor has a structure consisting predominantly of spherulitic ZrO_2 in glass, however it is apparent from the present study that, as the zircon feed particle size is reduced and the cooling rate increased, the spherulites become smaller and, in zircon rapidly quenched by spraying onto a cold substrate, they are no longer formed.

The spherulites have a branching non-crystallo-

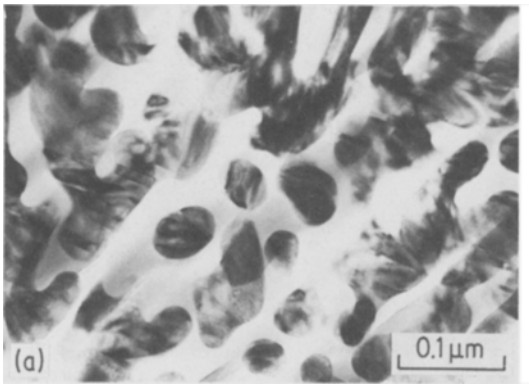

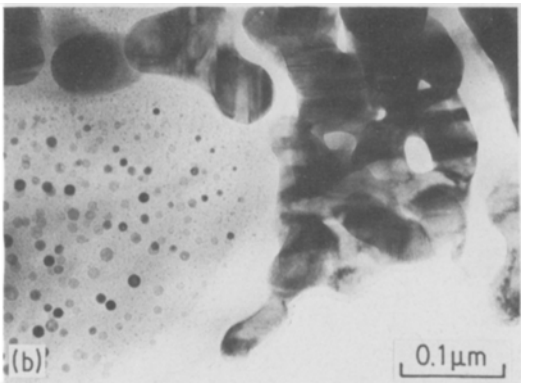

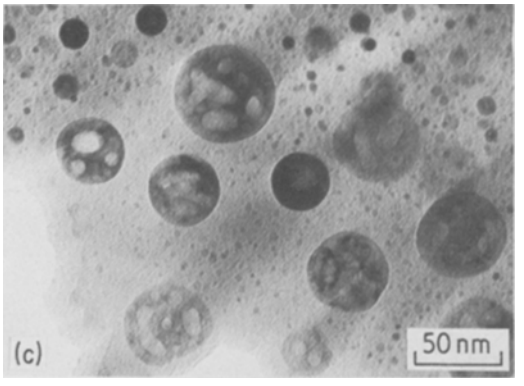

Figure 6 TEM, ion beam thinned specimen NPL PDZ.

graphic growth pattern, a type of structure which has been explained by Keith and Paddern [13] as arising from instability of growth of the original nucleus, when its diameter exceeds a certain value, as a result of a thin impurity-rich layer with thickness $\delta = D/G$ (where D is the diffusion coefficient and G is the growth rate) ahead of the growth interface. Spherulites branch to a limited extent at larger values of δ but at higher supercoolings (smaller δ), branching becomes more profuse to give compact spherulites. This theory was developed to explain spherulite crystallization of single component polymers and depends upon a small impurity concentration.

The main features of most of the spherulite observed by SEM in PDZ, are the presence of a more or less spherical "nucleus" at the centre with arms extending from it which branch at an increasing frequency, and decrease in width, as the spherulite radius increases. In many cases the outer edges of the spherulites seem to break up into separate small crystals (Figs. 3a and 3b). These observations suggest the following: ZrO_2 nuclei initially grow stably into the melt, to form spherical crystals, and the excess SiO_2 rejected accumulates ahead of the growing interface to form a thin layer of high viscosity (low D). This layer results in interface instability in the manner proposed by Keith and Paddern for their impurity layer so that fibrillar growth and non-crystallographic branching occur. The extent of branching is then controlled by the thickness of this boundary layer which depends upon its temperature and composition (controlling D) and the crystal growth rate (G). In some cases the process continues until spherulites meet (Fig. 2a), but in others spherulitic growth stops and some other process occurs (Fig. 2b). The fact that this latter effect is more common in the finer PDZ particles suggests that the temperature at the interface decreases to a value at which D in the boundary layer is so great that growth effectively ceases; a thin high-SiO_2 region is discernible surrounding the spherulites in many cases, for example, Fig. 2b, corresponding to this boundary layer.

The above considerations suggest that concentration gradients ahead of the growing spherulites do not extend over distances greater than $\sim 0.1\,\mu m$, implying that the bulk of the interspherulitic liquid remains at the $ZrSiO_4$ composition. The thermal history of particles during solidification will be controlled by the rate of evolution of the heat of fusion, and the rate at which heat is lost from the external surface. Remembering that nucleation will occur at considerable undercooling for isolated, completely molten particles, the crystal growth rate will be controlled by interface processes (in the present case, diffusion in the boundary layer) rather than heat flow considerations so that the rate of heat generation will be controlled by crystal growth rate unless the temperature rises to the liquidus. The thermal history of the solidifying droplet after nucleation

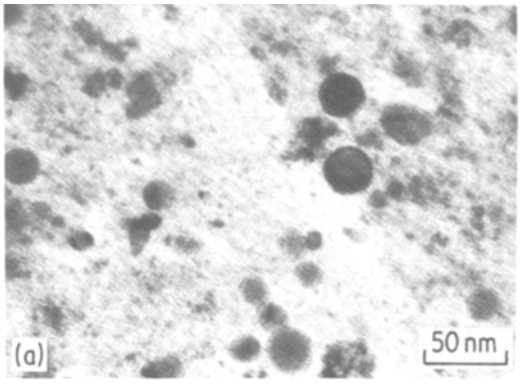

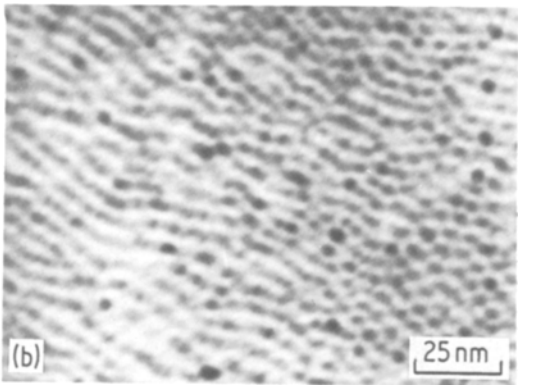

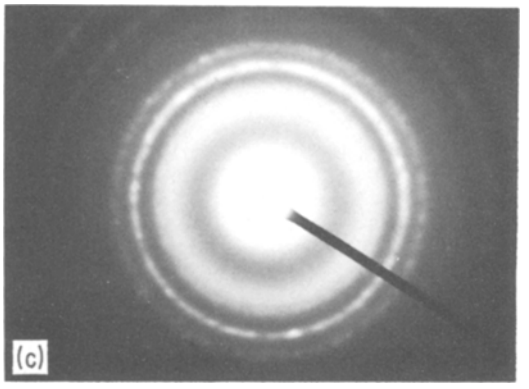

Figure 7 (a, b) TEM, ion beam thinned 6–10 μm fraction, laboratory prepared PDZ. (c) Selected area diffraction pattern, corresponding to 9b.

will therefore be strongly influenced by the droplet diameter, as discussed in detail for the case of Al_2O_3 [19]. Thus solidifying droplets may increase or decrease in temperature depending upon their size and surface heat transfer rate. For the reasons discussed above, however, the crystal growth rate for ZrO_2–SiO_2 liquid would be expected to be very much lower than for a single-component low-viscosity liquid, such as Al_2O_3, so that the temperature of the droplet would not be expected to rise very much or to decrease during crystallisation. The increased branching of the spherulites as their radius increases supports the latter view.

Spherulitic crystals constitute almost the only form of ZrO_2 present in large drops with low surface heat transfer rates because the temperature remains sufficiently high for this mode of crystal growth to occur at an appreciable rate. In smaller droplets (and/or higher heat transfer rates) the temperature decreases during spherulitic growth to the stage at which growth effectively ceases and the remaining liquid then solidifies by an alternative process. At the very high rates of heat transfer achieved by spraying onto a cold substrate, nucleation of primary ZrO_2 and its spherulitic growth are completely suppressed.

The above considerations apply to zircon particles which have completely melted. If melting is incomplete decomposition of residual zircon into $ZrO_2 + SiO_2$ glass at a relatively slow rate would be expected. This may be the origin of the irregular regions containing SiO_2-rich droplets observed in Fig. 3b.

There is a liquid miscibility gap in the SiO_2–ZrO_2 system [4] and this should, on theoretical grounds, be quite wide if extended into the low temperature metastable region [27]. The estimated miscibility gap is shown in Fig. 8 based on the liquidus data of Toropov and Galakhov [28] and the estimated width at half the consolute temperature [27].

It may be seen from Fig. 8 that liquid of the zircon composition would enter the miscibility gap on cooling, if crystallisation of ZrO_2 were suppressed. Thus phase separation would be possible in molten zircon quenched sufficiently rapidly to prevent nucleation of ZrO_2, or in regions between spherulites of spheroidized zircon which had cooled below a temperature at which crystal growth could occur at a reasonable rate. Homogeneous nucleation of liquid droplets from the liquid phase can occur much more readily than nucleation of crystals from the liquid because of the much lower interfacial energy between liquid phases [29] so that liquid–liquid phase separation could be expected at temperatures at which nucleation of crystalline phases would not take place, especially in high viscosity silicate liquids. The high ZrO_2 liquid phase would rapidly crystallise, however, because of the large decrease in D expected as the composition moved towards ZrO_2

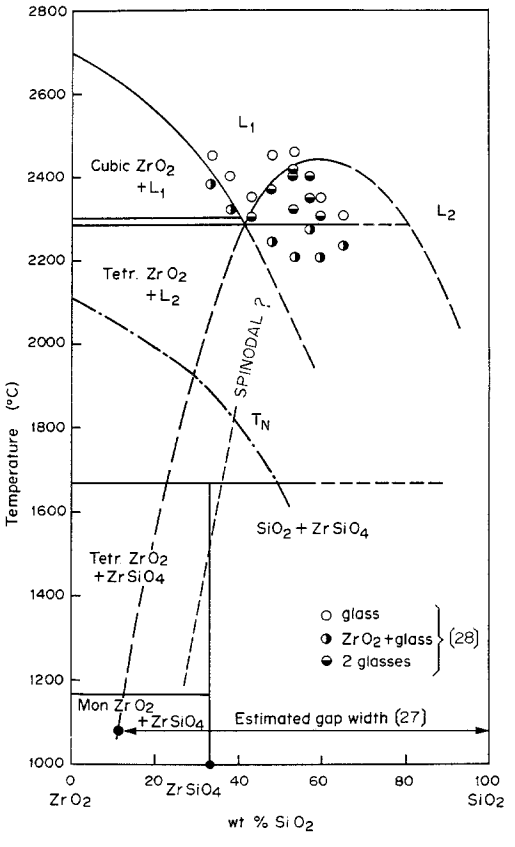

Figure 8 Phase diagram ZrO_2–SiO_2 system showing metastable miscibility region and spinodal (diagrammatic). T_N refers to estimated ZrO_2 nucleation temperature in isolated molten particles.

on cooling, whereas the SiO_2 rich phase would form a glass. The droplet microstructures observed (Figs. 6 and 7) between spherulites in PDZ are consistent with this explanation. The structure illustrated in Fig. 6c suggests several stages of phase separation, thus the large ZrO_2-enriched droplets initially formed later undergo further phase separation to give SiO_2-rich droplets within them. The matrix also undergoes further separation to produce ZrO_2-rich droplets in SiO_2 glass.

Close examination of the interspherulitic region in many cases reveals a bimodal distribution of ZrO_2 particles in SiO_2 glass (Figs. 6 and 7) with larger spherical particles ($\sim 0.1\,\mu m$) of the monoclinic phase and extremely small particles ($< 20\,nm$) of the tetragonal phase. There is evidence of a modulated structure in very thin regions (Fig. 7b). A modulated appearance is also apparent in rapidly quenched samples. This suggests a multistage process of decomposition of highly undercooled zircon-composition liquid and the modulated structures observed suggest spinodal decomposition. The microstructure shown in Fig. 7b in particular appears to consist of extremely small crystals of ZrO_2 within an amorphous, modulated structure. A possible explanation for this is that spinodal decomposition occurs as the critical temperature surface moves rapidly through the liquid, to form the linear pattern, and ZrO_2 crystallises from the ZrO_2 rich regions.

The glass transition temperatures (T_g) of silicate liquids, with higher liquidus temperatures, are approximately half the liquidus temperatures [30] giving a $T_g \sim 1100°$ C for compositions around zircon. There is thus a considerable temperature range (2400 to 1100° C) over which crystallization and phase separation could occur during cooling.

The plasma dissociation of zircon results from the fact that ZrO_2 crystallises from the melt during cooling and, for other than very slow cooling rates, the liquid phase forms SiO_2 glass and the zircon reassociation reaction does not occur. The variety of morphologies of ZrO_2 crystals observed in PDZ arise from alternative crystallization paths which depend upon undercooling. That is, direct nucleation and spherulitic growth from the liquid, and liquid phase separation or spinodal decomposition followed by crystallization from the ZrO_2-rich phase. In general all processes will occur sequentially in a single PDZ particle to give a complex microstructure.

5. Conclusions

The plasma dissociation of zircon into ZrO_2 crystals in SiO_2 glass results from the solidification processes occurring during cooling of molten zircon droplets. Spherulitic crystals of ZrO_2 are formed at high temperature by non-crystallographic branching because of a thin SiO_2 boundary layer at the crystal melt interface. At lower temperatures metastable liquid–liquid phase separation may occur followed by crystallization of ZrO_2 in the ZrO_2 rich regions. Phase separation may occur with a droplet morphology or as a very fine modulated structure probably associated with spinodal decomposition. The microstructure of individual PDZ particles can range from completely spherulitic, through mixed spherulitic–phase separated, to completely phase separated depending upon the cooling rate of the molten particles. Spherulitic ZrO_2 crystals have the monoclinic crystal structure but crystals smaller than $\sim 20\,nm$ diameter formed via phase separ-

ation retain the tetragonal form because of matrix restraint and interfacial energy effects.

Acknowledgements

This work has been supported by the Australian Research Grants Scheme and a Monash Special Research Grant. Thanks are also due to Mr R. K. Bayliss, National Physical Laboratory, UK, for samples of PDZ.

References

1. H. B. BARLETT, *J. Amer. Ceram. Soc.* **14** (1931) 837.
2. H. GEORGE and R. LAMBERT, *Compt. Rend. Acad. Sci.* 204 (1937) 688.
3. C. E. CURTIS and H. G. SOWMAN, *J. Amer. Ceram. Soc.* 36 (1953) 190.
4. W. C. BUTTERMAN and W. R. FOSTER, *Amer. Mineral* 52 (1967) 880.
5. I. H. WARREN and H. SHIMIZU, *Trans. Can. Inst. Min. Met.* 68 (1965) 169.
6. J. A. CHARLES, G. J. DAVIES, R. M. JERVIS and G. THURSFELD, *Trans. Inst. Min. Metall.* C79 (1970) 54.
7. P. H. WILKS, P. RAVINDER, C. L. GRANT, P. A. PELTON, R. J. DOWNER and M. L. TALBOT, *Chem. Eng. World* 9 (1974) 59.
8. R. K. BAYLISS, J. W. BRYANT and I. G. SAYCE, Proceedings of the 3rd International Symposium on Plasma Chemistry, Limoges, July 1977 (Université de Limoges, 1977) Paper S.5.2.
9. A. M. EVANS and J. P. H. WILLIAMSON, *J. Mater Sci.* 12 (1977) 779.
10. *Idem, ibid.* **14** (1979) 680.
11. A. M. EVANS, J. P. H. WILLIAMSON and F. P. GLASSER, *ibid.* 15 (1980) 2325.
12. AI MING WONG and R. McPHERSON, *ibid.* **16** (1981) 1732.
13. H. D. KEITH and F. J. PADDERN, *J. Appl. Phys.* 34 (1963) 2409.
14. R. C. GARVIE, *J. Phys. Chem.* 82 (1978) 218.
15. N. N. AULT, *J. Amer. Ceram. Soc.* 40 (1957) 69.
16. A. KRAUTH and H. MEYER, *Ber. Deutsch. Keram. Ges.* 42 (1965) 61.
17. T. OKUBO, O. YONEMOCHI, M. MAEDA and K. NAKAMURA, *Rep. Gov. Ind. Res. Inst. Nagoya* **16** (1967) 58.
18. R. McPHERSON, *J. Mater. Sci.* 8 (1973) 851.
19. R. McPHERSON and G. J. BAILEY, *ibid.* **16** (1981) 504.
20. R. C. GARVIE and P. S. NICHOLSON, *J. Amer. Soc.* 55 (1972) 303.
21. H. P. KLUG and L. E. ALEXANDER, "X-ray Diffraction Procedures for Polycrystalline and Amorphous Materials", (Wiley, New York, 1959).
22. E. D. WHITNEY, *Trans. Faraday Soc.* 61 (1965) 1991.
23. Y. MURASE and E. KATO, *J. Amer. Ceram. Soc.* 62 (1979) 527.
24. R. H. J. HANNINK, *J. Mater. Sci.* 13 (1978) 2487.
25. R. McPHERSON, B. V. SHAFER and A. M. WONG, *J. Amer. Ceram. Soc.* 65 (1982) C57.
26. N. CLAUSSEN, *ibid.* 61 (1978) 85.
27. F. YA GALAKHOV and G. G. VARSHAL, in "The Structure of Glass", Vol. 8, edited by E. A. Porai-Koshits (Consultants Bureau, New York, 1973) p. 7.
28. N. A. TOROPOV and F. YA GALAKHOV, *Bull. Acad. Sci. USSR Div. Chem. Sci.* 5 (1956) 153.
29. J. J. HAMMEL, *J. Chem. Phys.* 46 (1967) 2234.
30. S. SAKKA and D. McKENZIE, *J. Non-Cryst. Solids* 6 (1971) 145.

Received 28 November
and accepted 20 December 1983